J. Fluid Mech. (1990), *vol.* 211, *pp.* 355–372
Printed in Great Britain

Parallel flows with Soret effect in tilted cylinders

By DAVID JACQMIN
NASA Lewis Research Center, Cleveland, OH 44135, USA

(Received 10 January 1989 and in revised form 24 July 1989)

Henry & Roux have recently conducted extensive numerical studies on the interaction of Soret separation with convection in cylindrical geometry. Many of their solutions exhibit parallel flow away from endwalls. We show that their parallel flow results can be matched by closed-form solutions. We find that solutions are non-unique in some parameter regions. Disappearance of one branch of solutions correlates with a sudden transition of Henry & Roux's results from a separated to a well-mixed flow.

1. Introduction

A temperature gradient in a multicomponent fluid often tends to force gradients in composition. This is known as the Soret effect. Much experimental work has been carried out to determine Soret separations and coefficients in binary fluids. However, these experiments must contend with convective effects, which tend to mix the fluid. Convective transport can easily overwhelm diffusion in binary mixtures that have low molecular diffusivities.

Because of this problem with convection, there has been an interest in carrying out experiments in microgravity. Even then, though, convective effects are not necessarily negligible. Further, there is the problem that the orientation of the mean acceleration vector that forces convection is arbitrary and perhaps unknown.

Henry & Roux (1986, 1987, 1988) have recently carried out extensive numerical studies to evaluate the possible effects of steady microgravity accelerations. They considered convection–diffusion with Soret effect in a cylinder tilted at various angles to the acceleration. They determined the extent of modification of Soret separation by convection and determined regimes in which this modification is minimal. In their first paper they considered a horizontal cylinder at low Grashof numbers, in their second various angles of tilt at low Grashof numbers, and in their third a nearly vertical ('quasi-vertical') cylinder at Grashof numbers ranging from 482 to 4820. The Schmidt number for all their calculations was 60 and the Prandtl number 0.6. One of their most interesting results is that when the cylinder is quasi-vertical the transition from the separated to a well-mixed regime is very sudden, having the appearance of a bifurcation.

One prominent feature of most of their solutions is that they exhibit parallel flow away from the cylinder endwalls. This was apparent to Henry & Roux (hereinafter referred to as HR) and much of their analysis deals with the local force and mass balances of the parallel regime. However, they fail to take the next step of deriving parallel flow solutions.

This paper derives approximate parallel flow solutions that neglect convection by the secondary radial and azimuthal flows. Solutions are also simplified by treating the temperature as being imposed. This is generally acceptable for modelling HR's

results, which, partly because of their calculations' low Prandtl number, show a temperature field that is nearly linear and little affected by convection.

The result of greatest interest is that solutions can be non-unique. A parallel flow solution can be found for any given set of flow parameters and any given axial gradient of solute. However, for this solution to be relevant to cylinders with endwalls it must meet the condition of having no net solute flux. This condition adds significant nonlinearity to the problem. Different sets of flow parameters can yield different numbers of solutions. This turns out to be especially important for understanding the quasi-vertical case. Disappearance of one solution branch will be shown to correspond to a sudden transition in flow behaviour observed by HR. Non-unique solutions will also be shown to exist for the horizontal cylinder.

The paper proceeds as follows. We derive the parallel flow solutions and flux conditions in §2. Solutions for the axial solute gradient are discussed in §3, with results compared to those of HR. Emphasis will be put on discussing solution behaviour in parameter regions of non-uniqueness. Also, the boundaries of these regions will be determined.

2. Solution

We consider Boussinesq flow in a cylinder with radius R and length L. The aspect ratio L/R is $\gg 1$. We are interested in the flow away from the cylinder's endwalls, where the flow can be approximated as parallel. The cylinder is tilted at an angle γ, $-180° \leqslant \gamma \leqslant +180°$, to a steady acceleration vector $\boldsymbol{g}$. The $\gamma = 0°$ and $\pm 180°$ positions are vertical; $\gamma = \pm 90°$ is horizontal. $\gamma = 0°$ is the upward vertical position. Following HR, in the up (down) position the cylinder is heated from above (below). The temperature gradient in the down position is thus potentially unstable. Also following HR, 'quasi-vertical' refers only to angles of tilt near the up position. The flow has symmetry properties about $\gamma = 0°$ so there is no need to separately consider left and right positions. The coordinate system, which is the same as HR's, is shown in figure 1. The coordinates are arranged so that the axial coordinate increases downwards for $|\gamma| < 90°$ and so that the $\theta = 90°$ and 270° lines are in the horizontal plane.

The primary flow variables are the axial velocity w, the secondary radial and azimuthal flows u and v, the pressure p, and the solute concentration X. The temperature T is imposed. This amounts to approximating the flow's Prandtl number, $Pr = \nu/D_{TT}$, as being zero. Following HR, we take the relationship between density and temperature and concentration to be

$$\rho = \rho_0[1-\alpha(T-T_0)+\beta(X-X_0)].$$

The diffusive flux of solute is given by $-D_{TX}\nabla T - D_{XX}\nabla X$. D_{TX} is the Soret diffusion coefficient. The Boussinesq equations are non-dimensionalized by scaling length, velocity, temperature, and solute concentration by, respectively,

$$R, \quad \alpha|\boldsymbol{g}|R^3\left|\frac{\partial T}{\partial z}\right|/\nu, \quad R\left|\frac{\partial T}{\partial z}\right|, \quad R\left|\frac{\partial T}{\partial z}\right|D_{TX}/D_{XX}$$

The resulting non-dimensional parameters are the Grashof number $Gr = \alpha|\boldsymbol{g}|R^4|\partial T/\partial z|/\nu^2$, the Schmidt number $Sc = \nu/D_{XX}$, and $S = \beta D_{TX}/\alpha D_{XX}$. S relates the non-dimensional concentration gradient to the non-dimensional density gradient. We use the same symbols for non-dimensional as for dimensional variables. After non-dimensionalization, the imposed temperature equals $-z$.

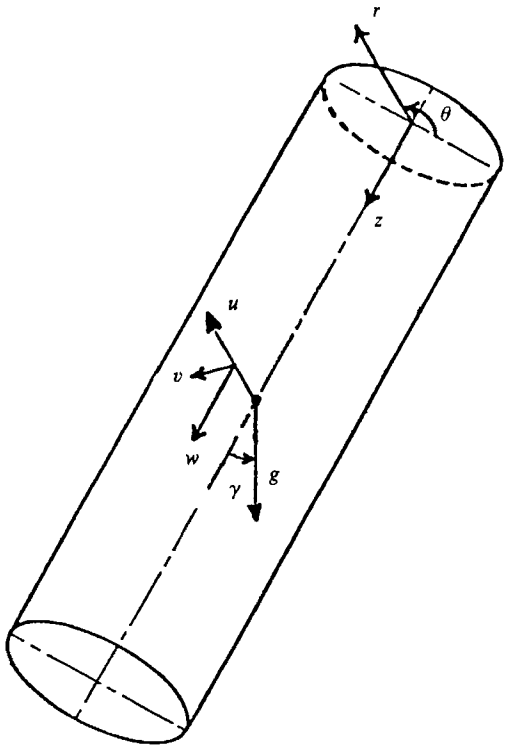

FIGURE 1. The coordinate system.

In order to obtain analytic solutions, it is necessary to simplify the Boussinesq equations by neglecting convection by the secondary radial and azimuthal flows. This is acceptable so long as these flows are 'small enough'. Their magnitude will be discussed after the flow field solutions are derived. However, we note now that the secondary flows are caused by $x = r\sin\theta$ gradients of density and that these gradients are usually quite small. In non-dimensional variables, the forcing of axial vorticity by these gradients is given by $-\sin\gamma S\,\partial X/\partial x$. HR give plots for the horizontally inclined cylinder that indicate an average $|\partial X/\partial x|$ of only about 0.015. For S positive, as the cylinder is moved towards the upward position the average $|\partial X/\partial x|$ becomes considerably smaller. This is because, as discussed by HR and for related problems by Hart (1971) and by Paliwal & Chen (1980), X then tends to a linear function of $y = r\cos\theta$ except in boundary layers at $r = 1$. These boundary layers become thinner as either S or the product $GrSc$ is increased.

With non-dimensionalization and after the above approximations, the Boussinesq equation set is

$$\frac{1}{r}\frac{\partial ru}{\partial r}+\frac{1}{r}\frac{\partial v}{\partial\theta}=0, \tag{2.1a}$$

$$-\frac{\partial p}{\partial z}+\cos\gamma(-T+SX)+\nabla^2 w=0, \tag{2.1b}$$

$$-\frac{\partial p}{\partial r}+\sin\gamma\cos\theta(-T+SX)+\nabla^2 u-\frac{u}{r^2}-\frac{2}{r^2}\frac{\partial v}{\partial\theta}=0, \tag{2.1c}$$

$$-\frac{1}{r}\frac{\partial p}{\partial \theta}-\sin\gamma\sin\theta(-T+SX)+\nabla^2 v-\frac{v}{r^2}-\frac{2}{r^2}\frac{\partial u}{\partial \theta}=0, \tag{2.1d}$$

$$Aw\frac{\partial X}{\partial z}=\nabla^2 X+\nabla^2 T, \tag{2.1e}$$

where $$\nabla^2=\frac{\partial^2}{\partial r^2}+\frac{1}{r}\frac{\partial}{\partial r}+\frac{1}{r^2}\frac{\partial^2}{\partial \theta^2}.$$

Exceptions to HR's notation in the above are that $Gr\,Sc$ is replaced by A and their unit acceleration vector $\tilde{\boldsymbol{g}}$ that multiplies $-T+SX$ is given in terms of its components $\{\cos\gamma, \sin\gamma\cos\theta, -\sin\gamma\sin\theta\}$. Again, the temperature is imposed as $T=-z$.

Neglect of convection by secondary flows partly decouples the system and allows solution in the form

$$w=\cos\theta\, w_1(r), \quad u=\cos 2\theta\, u_2(r), \quad v=\sin 2\theta\, v_2(r),$$

$$X=X_z z+\cos\theta X_1(r), \quad p=\cos\theta\, p_{rz} rz+p_{zz} z^2+p_0(r)+\cos 2\theta\, p_2(r).$$

The total concentration flux is given by

$$F=A\int_0^{2\pi}\int_0^1 \cos^2\theta\, w_1 X_1\, r\,\mathrm{d}r\,\mathrm{d}\theta-\pi(T_z+X_z). \tag{2.2}$$

This serves to fix X_z, since F must be zero for the solution to be relevant to a cylinder with endwalls. Setting $T_z=-1$, and after evaluation of the θ-integral, the no-flux condition becomes

$$X_z=1+A\int_0^1 w_1 X_1\, r\,\mathrm{d}r. \tag{2.3}$$

In the absence of convection, the unique solution from (2.3) is $X_z=-T_z=1$. This is the diffusion-dominated, Soret separated solution. However, this solution produces the density gradient $1+S$, so it is inconsistent with (2.1) except when $S=-1$ or when the cylinder is vertical.

We proceed now to the solution. The r and θ momentum equations give

$$p_{rz}=\sin\gamma(1+SX_z).$$

The z momentum equation then gives

$$p_{zz}=\tfrac{1}{2}\cos\gamma(1+SX_z).$$

The w_1 and X_1 equations become

$$\frac{\mathrm{d}^2 w_1}{\mathrm{d}r^2}+\frac{1}{r}\frac{\mathrm{d}w_1}{\mathrm{d}r}-\frac{1}{r^2}w_1+hX_1=qr, \tag{2.4a}$$

$$\frac{\mathrm{d}^2 X_1}{\mathrm{d}r^2}+\frac{1}{r}\frac{\mathrm{d}X_1}{\mathrm{d}r}-\frac{1}{r^2}X_1-sw_1=0, \tag{2.4b}$$

where $$h=\cos\gamma S, \quad q=\sin\gamma(1+SX_z), \quad s=AX_z.$$

Boundary conditions are that $w_1 = X_1 = 0$ at $r = 0$ and $w_1 = \mathrm{d}X_1/\mathrm{d}r = 0$ at $r = 1$.

Once X_1 is known, p_0, u_2, v_2 and p_2 can be determined from

$$\frac{\mathrm{d}p_0}{\mathrm{d}r} = \tfrac{1}{2}\sin\gamma S X_1, \tag{2.5a}$$

$$\frac{\mathrm{d}u_2}{\mathrm{d}r} + \frac{1}{r}u_2 + \frac{2}{r}v_2 = 0, \tag{2.5b}$$

$$\frac{\mathrm{d}^2u_2}{\mathrm{d}r^2} + \frac{1}{r}u_2 - \frac{5}{r^2}u_2 - \frac{4}{r^2}v_2 - \frac{\mathrm{d}p_2}{\mathrm{d}r} = -\tfrac{1}{2}\sin\gamma S X_1, \tag{2.5c}$$

$$\frac{\mathrm{d}^2v_2}{\mathrm{d}r^2} + \frac{1}{r}v_2 - \frac{5}{r^2}v_2 - \frac{4}{r^2}u_2 + \frac{2}{r}p_2 = +\tfrac{1}{2}\sin\gamma S X_1. \tag{2.5d}$$

In the present approximation u_2 and v_2 are not needed to determine X_z. We will derive them in order to determine the parameter ranges in which they are small.

2.1. *Cos γS positive*

The solution takes different forms depending on whether or not $\cos\gamma S$ is positive, zero, or negative. For $\cos\gamma S$ positive, solution is in terms of Kelvin functions. Then

$$w_1 = A\,\mathrm{ber}_1(mr) + B\,\mathrm{bei}_1(mr), \tag{2.6a}$$

$$X_1 = \frac{q}{h}r + \frac{m^2}{h}[A\,\mathrm{bei}_1(mr) - B\,\mathrm{ber}_1(mr)], \tag{2.6b}$$

$$A = -\frac{q}{m^3}\frac{\mathrm{bei}_1(m)}{\mathrm{ber}_1(m)\,\mathrm{ber}_1'(m) + \mathrm{bei}_1(m)\,\mathrm{bei}_1'(m)}, \tag{2.6c}$$

$$B = +\frac{q}{m^3}\frac{\mathrm{ber}_1(m)}{\mathrm{ber}_1(m)\,\mathrm{ber}_1'(m) + \mathrm{bei}_1(m)\,\mathrm{bei}_1'(m)}, \tag{2.6d}$$

where a prime indicates the derivative with respect to m, and $m = (|\cos\gamma S|\,AX_z)^{\frac{1}{4}}$. ($X_z$, as will be shown in §3, is positive, so m is real and positive.) The secondary flows are

$$u_2 = \tfrac{1}{4}\tan\gamma A(\mathrm{ber}_3(mr) + \mathrm{ber}_1(mr)) + \tfrac{1}{4}\tan\gamma B(\mathrm{bei}_3(mr) + \mathrm{bei}_1(mr)) - 2Cr^3 + 3Cr, \tag{2.7a}$$

$$v_2 = \tfrac{1}{4}\tan\gamma A(\mathrm{ber}_3(mr) - \mathrm{ber}_1(mr)) + \tfrac{1}{4}\tan\gamma B(\mathrm{bei}_3(mr) - \mathrm{bei}_1(mr)) + 4Cr^3 - 3Cr, \tag{2.7b}$$

$$C = -\tfrac{1}{4}\tan\gamma A\,\mathrm{ber}_3(m) - \tfrac{1}{4}\tan\gamma B\,\mathrm{bei}_3(m). \tag{2.7c}$$

The convective flux integral in (2.3) can be evaluated using formulae given in Abramowitz & Stegun (1964). We write the integral as

$$A\frac{q}{h}I_1 + B\frac{q}{h}I_2 + \frac{m^2}{h}(A^2 - B^2)I_3 + \frac{m^2}{h}ABI_4,$$

with

$$I_1 = \int_0^1 r^2\,\mathrm{ber}_1(mr)\,\mathrm{d}r = \frac{1}{m}\left(\mathrm{bei}_1' - \frac{1}{m}\mathrm{bei}_1\right), \tag{2.8a}$$

$$I_2 = \int_0^1 r^2\,\mathrm{bei}_1(mr)\,\mathrm{d}r = -\frac{1}{m}\left(\mathrm{ber}_1' - \frac{1}{m}\mathrm{ber}_1\right), \tag{2.8b}$$

$$I_3 = \int_0^1 r\,\mathrm{bei}_1(mr)\,\mathrm{ber}_1(mr)\,\mathrm{d}r = \tfrac{1}{4}(-\mathrm{ber}_0\,\mathrm{bei}_2 + 2\,\mathrm{ber}_1\,\mathrm{bei}_1 - \mathrm{ber}_2\,\mathrm{bei}_0), \tag{2.8c}$$

$$I_4 = \int_0^1 r(\mathrm{bei}_1^2(mr) - \mathrm{ber}_1^2(mr))\,\mathrm{d}r = \tfrac{1}{2}(\mathrm{bei}_1^2 - \mathrm{bei}_0\,\mathrm{bei}_2 - \mathrm{ber}_1^2 + \mathrm{ber}_0\,\mathrm{ber}_2). \tag{2.8d}$$

The argument (m) of the Kelvin functions on the right-hand side of (2.8) has been omitted for conciseness. Using

$$\mathrm{ber}_0 = -\frac{1}{\sqrt{2}}\left(\mathrm{ber}_1' - \mathrm{bei}_1' + \frac{1}{m}\mathrm{ber}_1 - \frac{1}{m}\mathrm{bei}_1\right),$$

$$\mathrm{bei}_0 = -\frac{1}{\sqrt{2}}\left(\mathrm{ber}_1' + \mathrm{bei}_1' + \frac{1}{m}\mathrm{ber}_1 + \frac{1}{m}\mathrm{bei}_1\right),$$

$$\mathrm{ber}_2 = +\frac{1}{\sqrt{2}}\left(\mathrm{ber}_1' - \mathrm{bei}_1' - \frac{1}{m}\mathrm{ber}_1 + \frac{1}{m}\mathrm{bei}_1\right),$$

$$\mathrm{bei}_2 = +\frac{1}{\sqrt{2}}\left(\mathrm{ber}_1' + \mathrm{bei}_1' - \frac{1}{m}\mathrm{ber}_1 - \frac{1}{m}\mathrm{bei}_1\right),$$

the flux equation becomes

$$X_z = 1 - \frac{\tan^2\gamma(1+SX_z)^2}{S^2X_z}\left(\frac{5}{4} - \frac{1}{4}\frac{q_1^2}{r_1^2} - \frac{1}{m}\frac{p_1}{r_1} - \frac{1}{4}\frac{1}{m^2}\frac{p_1^2}{r_1^2}\right)$$

$$= 1 - \frac{\tan^2\gamma(1+SX_z)^2}{S^2X_z}\,\Psi_+(m). \tag{2.9}$$

p_1, q_1, and r_1 are monotonically increasing Kelvin function cross-products (the notation follows Abramowitz & Stegun). For general order ν they, along with one other cross-product s_ν, are

$$p_\nu = \mathrm{ber}_\nu^2 + \mathrm{bei}_\nu^2, \quad q_\nu = \mathrm{ber}_\nu\,\mathrm{bei}_\nu' - \mathrm{bei}_\nu\,\mathrm{ber}_\nu',$$

$$r_\nu = \mathrm{ber}_\nu\,\mathrm{ber}_\nu' + \mathrm{bei}_\nu\,\mathrm{bei}_\nu', \quad s_\nu = \mathrm{ber}_\nu'^2 + \mathrm{bei}_\nu'^2.$$

Recursion relationships (Abramowitz & Stegun) for these cross-products can be manipulated to give p_1, q_1, and r_1 in terms of q_0, r_0, and s_0:

$$p_1 = s_0, \quad q_1 = r_0, \quad r_1 = q_0 - \frac{1}{m}s_0.$$

The advantage of these latter cross-products is that they are somewhat more thoroughly documented and described in the mathematical literature.

The various Kelvin function cross-products needed to evaluate $\Psi_+(m)$ can be calculated using Taylor series given by Abramowitz & Stegun. Numerical evaluation of the series is straightforward and turns out to be quite efficient. For small m, some algebra (using MACSYMA) yields

$$\Psi_+(m) \approx \frac{\frac{7}{46080}m^8 + \frac{23}{82575360}m^{12} + \frac{77}{407686348800}m^{16}}{1 + \frac{1}{32}m^4 + \frac{5}{18432}m^8 + \frac{91}{212336640}m^{12}} \tag{2.10}$$

or, more roughly,

$$\Psi_+(m) \approx \frac{7}{46080}m^8 - \frac{41}{9175040}m^{12}. \tag{2.11}$$

Remembering that $m = (|\cos\gamma S|X_z\Lambda)^{\frac{1}{4}}$, equation (2.9) can be approximated using (2.11) as

$$X_z \approx 1 - \Lambda^2\sin^2\gamma(1+SX_z)^2X_z\left(\frac{7}{46080} - \frac{41}{9175040}\cos\gamma S\Lambda X_z\right). \tag{2.12}$$

m	$\Psi_+(m)$	Equation (2.10)	Equation (2.11)	Equation (2.13)
0	0	0	0	
0.5	5.923×10^{-7}	5.923×10^{-7}	5.923×10^{-7}	—
1.0	1.475×10^{-4}	1.475×10^{-4}	1.475×10^{-4}	—
1.5	3.372×10^{-3}	3.372×10^{-3}	3.313×10^{-3}	—
2.0	2.548×10^{-2}	2.548×10^{-2}	2.058×10^{-2}	—
2.5	9.352×10^{-2}	9.354×10^{-2}	—	—
3.0	0.2077	0.2081	—	0.2441
3.5	0.3342	0.3365	—	0.3724
4.0	0.4409	0.4545	—	0.4643
4.5	0.5225	0.5629	—	0.5331
5.0	0.5825	0.6756	—	0.5864
6.0	0.6630	—	—	0.6637
8.0	0.7550	—	—	0.7556
10.0	0.8079	—	—	0.8082
15.0	0.8754	—	—	0.8755
20.0	0.9078	—	—	0.9079
30.0	0.9394	—	—	0.9394
∞	1.0	—	—	1.0

TABLE 1. $\Psi_+(m)$ and approximations to $\Psi_+(m)$

For large m, Abramowitz & Stegun give asymptotic series in inverse powers of m for the cross-products q_0, r_0 and s_0. From these we obtain, to order $1/m^2$,

$$\Psi_+(m) \approx 1-\frac{5\sqrt{2}}{4}\frac{1}{m}-\frac{3}{2}\frac{1}{m^2}. \tag{2.13}$$

Table 1 compares the exact $\Psi_+(m)$ to the large-m and the two small-m approximations. The large-m approximation is useful for qualitative purposes down to $m = 2.6$ and accurate to two figures at $m = 5$. Equation (2.10) is accurate up to $m = 3.6$, while (2.11) is accurate up to about $m = 1.6$.

2.2. *Cos γ S zero*

When $\cos\gamma S = 0$ equations (2.4*a*, *b*) decouple. Then

$$w_1 = \tfrac{1}{8}\sin\gamma(1+SX_z)(r^3-r) \tag{2.14a}$$

$$X_1 = \tfrac{1}{8}\sin\gamma\,\Lambda X_z(1+SX_z)(\tfrac{1}{24}r^5-\tfrac{1}{8}r^3+\tfrac{1}{6}r). \tag{2.14b}$$

The secondary flows are

$$u_2 = \tfrac{1}{8}\sin\gamma(1+SX_z)\,\tfrac{1}{48}\sin\gamma\,\Lambda X_z S(-\tfrac{1}{240}r^7+\tfrac{1}{32}r^5-\tfrac{1}{20}r^3+\tfrac{11}{480}r), \tag{2.15a}$$

$$v_2 = \tfrac{1}{8}\sin\gamma(1+SX_z)\,\tfrac{1}{48}\sin\gamma\,\Lambda X_z S(-\tfrac{1}{60}r^7-\tfrac{3}{32}r^5+\tfrac{1}{10}r^3-\tfrac{11}{480}r). \tag{2.15b}$$

The flux equation is

$$X_z = 1-\frac{7\Lambda^2\sin^2\gamma(1+SX_z)^2}{46080}X_z \tag{2.16}$$

valid for $\sin^2\gamma = 1$, or $S = 0$, or both. Equations (2.14)–(2.16) could also have been derived from equations (2.6)–(2.7), (2.9), (2.11) for $m\to0$.

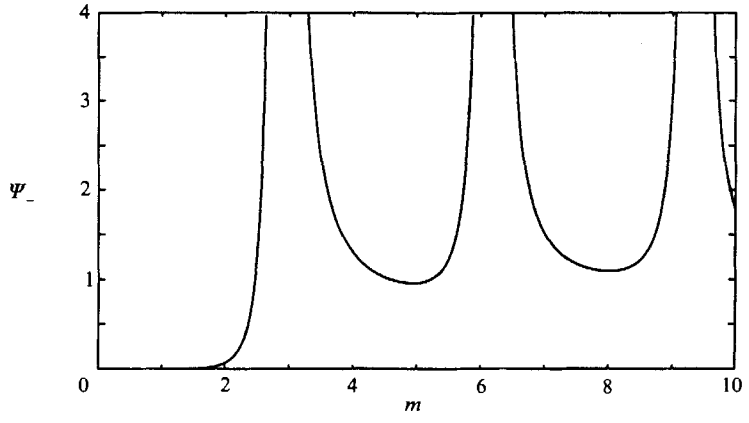

FIGURE 2. $\Psi_-(m)$.

2.3. *Cos γS negative*

When $\cos\gamma S$ is negative, solution is in terms of Bessel functions. Then

$$w_1 = AJ_1(mr)+BI_1(mr), \tag{2.17a}$$

$$X_1 = \frac{q}{h}r+\frac{m^2}{h}[AJ_1(mr)-BI_1(mr)], \tag{2.17b}$$

$$A = -\frac{q}{m^3}\frac{I_1(m)}{J_1(m)I_1'(m)+J_1'(m)I_1(m)}, \tag{2.17c}$$

$$B = +\frac{q}{m^3}\frac{J_1(m)}{J_1(m)I_1'(m)+J_1'(m)I_1(m)}. \tag{2.17d}$$

The secondary flows are

$$u_2 = \tfrac{1}{4}\tan\gamma A(J_3(mr)+J_1(mr))-\tfrac{1}{4}\tan\gamma B(I_3(mr)-I_1(mr))-2Cr^3+3Cr, \tag{2.18a}$$

$$v_2 = \tfrac{1}{4}\tan\gamma A[J_3(mr)-J_1(mr)]-\tfrac{1}{4}\tan\gamma B[I_3(mr)+I_1(mr)]+4Cr^3+3Cr, \tag{2.18b}$$

$$C = -\tfrac{1}{4}\tan\gamma AJ_3(m)+\tfrac{1}{4}\tan\gamma BI_3(m). \tag{2.18c}$$

The flux equation is

$$X_z = 1-\frac{\tan^2\gamma(1+SX_z)^2}{S^2X_z}\left(1+\frac{1}{2}\frac{J_1^2I_1'^2+J_1'^2I_1^2}{W^2}-\frac{2}{m}\frac{J_1I_1}{W}-\frac{1}{2}\frac{1}{m^2}\frac{J_1^2I_1^2}{W^2}\right)$$

$$= 1-\frac{\tan^2\gamma(1+SX_z)^2}{S^2X_z}\Psi_-(m), \tag{2.19}$$

where the argument (m) is omitted and where W equals $J_1I_1'+J_1'I_1$.

$\Psi_-(m)$ is shown in figure 2. It is infinite at the zeros of W. The first four zeros are at $m \approx 2.87$, 6.145, 9.335, and 12.495, intervals between zeros asymptoting to π. (The zeros correspond to eigenfunctions for the vertical case, each indicating the onset of an unstable mode.) Ψ_-, like Ψ_+, is always positive. Ψ_- tends with increasing m to a minimum value of $\frac{5}{4}$. Equations (2.10) and (2.11) modified by $-m^4$ substituted for m^4 can be used to approximate Ψ_- for small m. Also, (2.12) holds as written for both positive and negative $\cos\gamma S$. The modified (2.10) is accurate for m up to about 2.6 and qualitatively correct to its denominator's first zero (which occurs at $m \approx 2.82$). The modified (2.11) is accurate up to $m \approx 1.4$.

2.4. *The velocity fields*

The solution for X is valid only as long as u_2 and v_2 are small compared to w_1. Further, they should be small in absolute terms. In this section we establish ranges of γ and Λ in which these criteria are met.

We first discuss some overall characteristics of the velocity fields. For $\cos\gamma S$ positive and m large, w_1 is concentrated near the cylinder boundary. The width of its boundary current is $O(1/m)$. The maximum value of $|w_1|$ in the current is proportional to $1/m^3$ while outside of the current w_1 has an exponentially decaying dependence on m. $|w_1|_{\max}$ is quite small. For example, for $m = 10$ it is only about $5\times10^{-4}|q|$. X_z, as will be shown in the next section, is limited to the range 0 to 1 and, following HR, we will only consider $|S| \leqslant 1$. Thus, $|q|$ is $O(|\sin\gamma|)$. The azimuthal velocity v_2 also exhibits boundary-layer behaviour. It and u_2 are larger in the interior than w_1 because of their polynomial dependence there. The maximum amplitudes of both, like w_1, exhibit a $1/m^3$ dependence. At large m the maximum $|u_2|$ and $|v_2|$ are $O(|\tan\gamma\|w_1|_{\max})$. Thus, both are much smaller than $|w_1|_{\max}$ when $|\gamma|$ is near 0° or $\pm180°$. The radial velocity u_2 does not exhibit boundary-layer behaviour and is weak near $r = 1$. This can be seen in (2.7*a*) when one realizes that $\mathrm{ber}_3(mr)$ and $\mathrm{bei}_3(mr)$ approximately cancel $\mathrm{ber}_1(mr)$ and $\mathrm{bei}_1(mr)$ when mr is large.

For $\cos\gamma S$ negative with m large, the velocities are greatest near the cylinder centre. For example, except near $r = 1$, w_1 behaves like $J_1(mr)$, which at large mr decays like $1/(mr)^{\frac{1}{2}}$. The $|w_1|$ maximum is near the maximum of $J_1(mr)$ at $mr \approx 2$. The magnitudes of the three velocities oscillate with m but the general trend, as for the $\cos\gamma S$ positive case, is a $1/m^3$ decay. Except near 'resonance', values of m (the zeros of W) these velocities are small. For example, at $m = 10$, $|w_1|_{\max} \approx 3\times10^{-3}|q|$. As with $\cos\gamma S$ positive, $|u_2|_{\max}$ and $|v_2|_{\max}$ are $O(|\tan\gamma\|w_1|_{\max})$.

For $\cos\gamma S$ zero

$$|w_1|_{\max} \approx 0.048|q|, \quad |u_2|_{\max} \approx 1.65\times10^{-5}|\sin\gamma\Lambda X_z Sq|,$$
$$|v_2|_{\max} \approx 1.50\times10^{-5}|\sin\gamma\Lambda X_z Sq|.$$

These magnitudes hold approximately for $\cos\gamma S$ non-zero for m up to about 2. For comparison with the order of magnitude relationships given in the previous paragraphs, $|\sin\gamma\Lambda X_z S| = m^4|\tan\gamma|$.

From the above, it is apparent that for any m there are two ranges of γ, centred on $\gamma = 0°$ and $\pm180°$, such that u_2 and v_2 are small compared to w_1. We have considered two measures of velocity magnitudes. The first, used above, compares maximum amplitudes. The second compares integrals of the velocities' absolute values. Writing w_1 as $q\tilde{w}(mr)$ and $\{u_2, v_2\}$ as $\tan\gamma\, q\{\tilde{u}(mr), \tilde{v}(mr)\}$, we want, for the first measure,

$$|\tan\gamma|\frac{|\tilde{u}|_{\max}}{|\tilde{w}|_{\max}} \leqslant \epsilon, \quad |\tan\gamma|\frac{|\tilde{v}|_{\max}}{|\tilde{w}|_{\max}} \leqslant \epsilon.$$

For the second measure, we want

$$|\tan\gamma|\frac{\int_0^1 r|\tilde{u}|\,\mathrm{d}r}{\int_0^1 r|\tilde{w}|\,\mathrm{d}r} \leqslant \epsilon, \quad |\tan\gamma|\frac{\int_0^1 r|\tilde{v}|\,\mathrm{d}r}{\int_0^1 r|\tilde{w}|\,\mathrm{d}r} \leqslant \epsilon.$$

We define $|\gamma|_{\max}(m, \epsilon)$ as the maximum deviation of the cylinder from the up or down positions such that either set of constraints is met. Table 2 gives $|\gamma|_{\max}$ for $\epsilon = 0.1$ for

m	$\lvert\tilde{w}\rvert_{\max}$	$\lvert\gamma\rvert_{\max}$, maximum (degrees)	$\lvert\gamma\rvert_{\max}$, integral (degrees)
		$\cos\gamma S > 0$	
1	4.7×10^{-2}	89.8	89.8
2	3.9×10^{-2}	86.9	87.5
4	9.6×10^{-3}	52.5	58.5
6	2.6×10^{-3}	24.8	25.5
8	1.0×10^{-3}	17.3	15.7
10	5.2×10^{-4}	14.7	12.3
12	2.9×10^{-4}	13.4	10.6
16	1.2×10^{-4}	12.2	9.1
20	6.1×10^{-5}	11.8	8.4
		$\cos\gamma S < 0$	
1	4.9×10^{-2}	89.8	89.8
2	6.4×10^{-2}	86.9	87.5
4	2.1×10^{-2}	48.0	51.0
6	4.5×10^{-3}	17.4	14.8
8	3.1×10^{-3}	15.4	17.7
10	2.8×10^{-3}	16.6	12.5
12	2.3×10^{-3}	17.7	12.7
16	1.5×10^{-3}	18.0	11.9
20	3.2×10^{-4}	17.6	11.8

TABLE 2. $\lvert\tilde{w}\rvert_{\max}$ and $\lvert\gamma\rvert_{\max}$ as functions of m. $\epsilon = 0.1$

both amplitude measures. $\lvert\tilde{w}\rvert_{\max}$ is also given. For $\cos\gamma S$ positive, $\lvert\gamma\rvert_{\max}$ decreases monotonically with increasing m, asymptoting to about 11.2° with the maximum measure or 7.7° by the integral measure. For $\cos\gamma S$ negative, $\lvert\gamma\rvert_{\max}$ is oscillatory. As m increases, the oscillations become smaller, centring near 18° (maximum measure) or 12° (integral measure). By both measures, then, there is a range of γ for which u_2 and v_2 are small compared with w_1 for all m. In particular, HR's quasi-vertical case ($\gamma \approx 1°$) is well within this range.

In the vicinity of m equal to zero $\lvert\gamma\rvert_{\max}$ equals $90°-O(m^4)$. At 90° itself it is necessary to look at relative magnitudes in terms of Λ. Then $\lvert u_2\rvert_{\max}$ and $\lvert v_2\rvert_{\max}$ are about $3\times10^{-4}\Lambda X_z\lvert S\rvert\lvert w_1\rvert_{\max}$. For ϵ to be less than $0.1\,\Lambda X_z\lvert S\rvert$ can thus range up to about 300. All HR's calculations of $\Lambda X_z\lvert S\rvert$ fall well below this.

The above discussion is subject to one important caveat. When $\lvert\gamma\rvert > 90°$ the cylinder is heated from below. Convection can readily distort the temperature field for this case when $GrPr$ is large. The approximation used herein of a fixed temperature field is then invalid. Large m, of course, implies large Gr. Our discussion of the flow at large m appears to be applicable generally for $\lvert\gamma\rvert < 90°$ but is restricted to only small Pr for $\lvert\gamma\rvert > 90°$.

3. Results from the flux equations

We will be comparing our solutions for X_z to those of HR and some comments are needed on how this is done. HR's numerical work was done for cylinders with lengths (aspect ratios) of from 3 up to 12. Almost all of their computations show sizable parallel flow regions away from the cylinder endwalls. The one major exception is for $S \leqslant 0.02$ for their quasi-vertical study. A cylinder length of 3 was used for the quasi-vertical case and it is apparently too short to exhibit a parallel flow region when S

is small. All HR's studies present graphs of $X(z)$ at $r = 0$ for various A, S, and γ. Rough approximations to their calculated mid-cylinder X_z can be determined from them. A more accurate method of determining their X_z is available for HR's low Grashof number studies. For those, HR plot mid-cylinder X_z as a function of maximum parallel flow velocity. They then separately plot this velocity as a function of A, S, and γ. In both cases, data points as well as interpolatory curves are plotted. We found it possible to relate data points on the two plots and thus directly find their $X_z(A, S, \gamma)$.

3.1. *General comments on the solution*

The fact that $\Psi_\pm$ is positive has important consequences for solutions to (2.9), (2.19). From it, X_z must also be positive – and from that, $0 \leqslant X_z \leqslant 1$. The m^8 dependence of $\Psi_\pm$ at small m means that the right-hand sides of (2.9)–(2.19) are 1 when X_z equals zero. When $X_z = 1$ the right-hand sides are less than one. Thus, there must be at least one solution and the number of solutions must be odd.

The most effective solution procedure for (2.9)–(2.19) is to choose m, evaluate $\Psi_\pm(m)$ and then find X_z as a function of S and γ from the resulting quadratic equation. This gives

$$X_z = \frac{1}{2}\frac{S-2G}{S(1+G)} \pm \left(\frac{1}{4}\frac{(S-2G)^2}{S^2(1+G)^2} - \frac{G}{S^2(1+G)}\right)^{\frac{1}{2}}, \tag{3.1}$$

where $G(\gamma, m) = \tan^2\gamma\, \Psi_\pm(m)$. Once X_z is found, A can then be found from m as $A = m^4/|\cos\gamma S| X_z$. There are no solutions to (3.1) in the range

$$2G - (4G^2+4G)^{\frac{1}{2}} < S < 2G + (4G^2+4G)^{\frac{1}{2}} \tag{3.2}$$

or for

$$(S+1)\,G > \tfrac{1}{4}S^2.$$

At the double root of (3.1), $X_z = 1/(S+2)$. There are always solutions to (3.1) when $S \leqslant -1$.

We now consider solutions for $A \to \infty$. This is helpful for understanding the overall solution structure. One solution is then always $X_z \approx 0$, $m \approx 0$. More specifically,

$$X_z \approx \frac{46080}{7\sin^2\gamma A^2}, \quad \text{while} \quad m \approx \left(\frac{46080|\cos\gamma S|}{7\sin^2\gamma A}\right)^{\frac{1}{4}}.$$

Additional solutions, if they exist, are for $m \to \infty$. For the case of $\cos\gamma S$ positive, $\Psi_+ \to 1$ and $G \to \tan^2\gamma$. Multiple solutions exist if

$$S \leqslant 2\tan^2\gamma - (4\tan^4\gamma + 4\tan^2\gamma)^{\frac{1}{2}} \tag{3.3a}$$

or

$$S \geqslant 2\tan^2\gamma + (4\tan^4\gamma + 4\tan^2\gamma)^{\frac{1}{2}}. \tag{3.3b}$$

Satisfaction of either constraint leads to a total of three solutions, as $A \to \infty$, for a given A. For $\cos\gamma S$ negative, Ψ_- does not converge to any value but it does go to a minimum value of $\frac{5}{4}$. Then multiple solutions can occur when

$$S \leqslant \tfrac{5}{2}\tan^2\gamma - (\tfrac{25}{4}\tan^4\gamma + 5\tan^2\gamma)^{\frac{1}{2}} \tag{3.4a}$$

$$S \geqslant \tfrac{5}{2}\tan^2\gamma + (\tfrac{25}{4}\tan^4\gamma + 5\tan^2\gamma)^{\frac{1}{2}}. \tag{3.4b}$$

As $\gamma \to \frac{1}{2}\pi$, bounds (3.3*a*) and (3.4*b*) approach $S \leqslant -1$. Because of the oscillations of Ψ_-, it appears possible that satisfaction of (3.4) may lead, as $A \to \infty$, to an infinite number of solutions.

A similar caveat exists for this section as for §2.4. Bounds (3.3*a*) and (3.4*b*) are for the heated-from-below case. They are most likely applicable only for $Pr \to 0$.

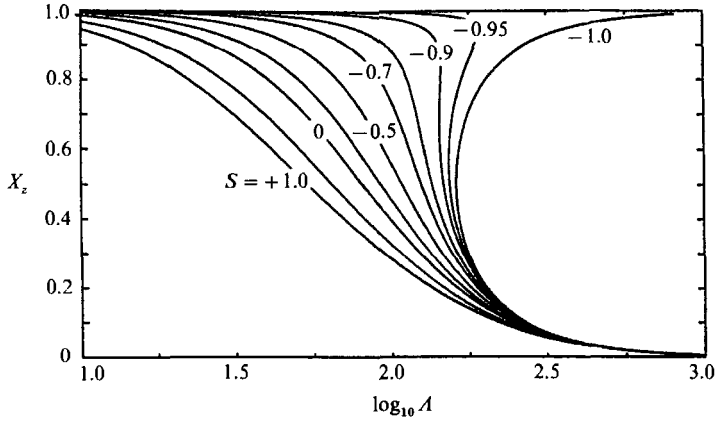

FIGURE 3. $X_z(A)$ for the horizontal case for S equal to $+1.0$, $+0.5$, 0, -0.25, -0.5, -0.7, -0.8, -0.9, -0.95, and -1.

3.2. *The case* $\cos\gamma S = 0$

When $S = 0$

$$X_z = \frac{1}{1 + \dfrac{7A^2 \sin^2\gamma}{46080}}. \tag{3.5}$$

When the cylinder is horizontal

$$X_z = \frac{1}{1 + \dfrac{7A^2(1+SX_z)^2}{46080}}. \tag{3.6}$$

The second case could be written and solved as a cubic equation. The above form, however, is useful for iterative calculations when S is positive. The right-hand side of (3.6) then decreases monotonically with increasing X_z and there is necessarily only one real solution.

Figure 3 shows X_z as a function of A for various $|S| \leqslant 1$. To have three real solutions, it turns out that S must be less than -0.89. The minimum A for this to occur is about 140.9. At $S = -1$ the threshold A is $(\frac{184320}{7})^{\frac{1}{2}} \approx 162.3$. As $A \to \infty$ there are, in agreement with (3.4), three real solutions only for $S \leqslant -1$. (For $S = -1$ one of the three solutions is identically $X_z = 1$). Where there are multiple solutions, the middle solution, in terms of ordering by X_z, is probably unstable. The upper solution, consistent with the degree of Soret separation, has the lowest rate of flow and the lower solution has the highest. It would be interesting to find out if the upper and lower solutions are stable over a common range of A. HR's work for the horizontal case was limited to $S \geqslant -0.75$ so they had no chance to observe any non-uniqueness phenomena.

Our results for the horizontal case are very close to HR's. For example, for $A = 60$, $S = -0.5$, equation (3.6) gives $X_z = 0.846$, while HR obtained about 0.85. For $A = 120$, $S = 0.5$, (3.6) gives 0.263, while HR obtained 0.26. Table 3 gives additional comparisons.

The solution for the case $S = 0$ is exact (since then there are no secondary flows). Results are again very close to those of HR. For $A = 60$ with the cylinder horizontal, (3.5) gives $X_z = 0.646$, while HR obtained about 0.63. At $\gamma = 45°$ and $A = 60$ (3.5) gives $X_z = 0.785$ while HR obtained about 0.78. Again, table 3 gives additional comparisons.

γ (degrees)	A	S	X_z(HR)	X_z(J)
135	60	0.5	0.58	0.591
135	60	−0.5	0.95	0.958
135	180	0.5	0.17	0.185
135	180	−0.5	0.74	0.752
90	60	0.5	0.52	0.533
90	180	−0.5	0.18	0.201
90	180	0.5	0.14	0.15
45	60	−0.5	0.85	0.857
45	60	0.5	0.75	0.746
45	180	−0.5	0.22	0.239
45	180	0	0.27	0.289
45	180	0.5	0.32	0.34
22.5	60	−0.5	0.96	0.943
22.5	60	0.5	0.93	0.917
22.5	180	−0.5	0.37	0.376
22.5	180	0	0.58	0.581
22.5	180	0.5	0.73	0.726
1.0	28920	0.02	<0.4	0.049
1.0	16800	0.02		0.4
1.0	289200	0.05	0.88	0.902
1.0	289200	0.1	0.97	0.973

TABLE 3. Comparison of HR's results (HR) to the present ones (J) for X_z, for various γ, A, and S. HR's results were read from charts and are given only approximately. HR's results for $A = 28920$ are for non-parallel flow.

3.3. *The quasi-vertical case: positive S*

For this case, HR considered flow for A up to 2.892×10^5 ($Gr = 4820$), with m ranging up to about 20. m is large enough to use the large-m approximation (2.13) or, for qualitative purposes, Ψ_+ can be approximated simply as 1. As implied by the bounds (3.3) and (3.4), the quasi-vertical case has significant regimes of non-uniqueness. A jump from one solution to another will be shown to explain some of HR's results.

For the quasi-vertical case, $\tan\gamma$ can be approximated as γ. Approximating Ψ_+ as 1 and using $\gamma \ll 1$, (3.1) simplifies to

$$X_z = \tfrac{1}{2} \pm \left(\frac{1}{4} - \frac{\gamma^2}{S^2}\right)^{\frac{1}{2}}. \tag{3.7}$$

The cutoff for large-m solutions is thus at $S \approx 2\gamma$. This cutoff can be matched to one result of HR. HR's quasi-vertical numerical calculations were restricted to $\gamma = 1°$. In their large-A calculations they observed a sudden transition from large to small X_z as S decreased below about 0.03. Equation (3.7) predicts the disappearance of the large-m solution – and, thus, a discontinuous transition to small X_z – at $S = 0.0349$.

This estimate of the transition S can be improved by use of the large-m approximation given by (2.13). In HR's large-A calculations m at the transition is about 8.11. Equation (2.13) can be applied to (3.7) by modifying γ^2 to $\gamma^2\Psi_+(m)$. We then obtain a transition S of 0.0304. Finally, the exact equation (3.2) yields 0.0309. These are now in very close agreement with HR's numerical results.

Equations (2.13), (3.7), (3.2) also give similar results to HR for larger S. For example, for $S = 0.05$, for the large-A calculation, HR obtained $X_z \approx 0.88$: m is then about 10.6. Equations (2.13), (3.7) yield $X_z \approx 0.887$ and (3.2) gives 0.902.

Figure 4 shows solution curves calculated from the exact equation (2.9). Multiple

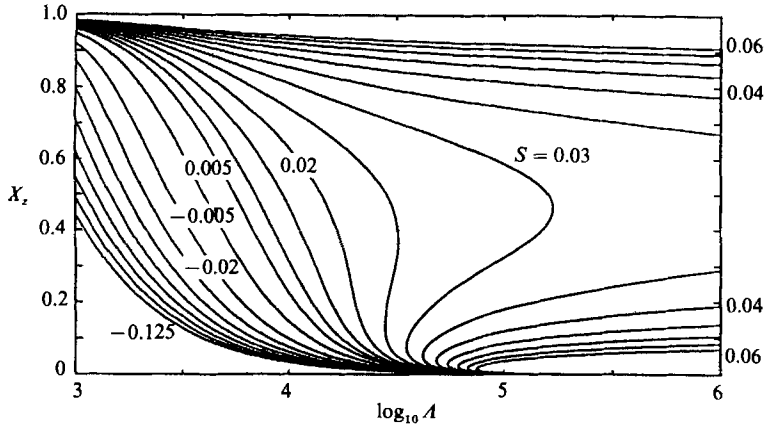

FIGURE 4. $X_z(A)$ for $\gamma = 1°$ for S equal to -0.125 to -0.005 by intervals of 0.015, and 0.005 to 0.06 by intervals of 0.005. For negative S, solutions are shown only for $m < 2.87$ (up to the first zero of W).

solutions can occur for S greater than about 0.023. As with the horizontal case (and as is always true) the lower the solution branch the greater the flow rate.

Figure 4 is in good agreement with HR's (1988) figure 10 except for small S in the neighbourhood of A equal to 20000. In that region the flow exhibits a sharp, continuous transition from significant to small separation with increasing A. The present calculations indicate this transition takes place for a smaller A than do HR's. For example, for $S = 0.02$ HR calculate the centre of the transition to be at $A \approx 25000$ while we find the centre at about 15000. Part of the discrepancy is due to the small aspect ratio that HR chose for their quasi-vertical calculations. In their small-S calculations the resulting flow is not quite parallel even at mid-cylinder. Endwall effects are important throughout the cylinder and these increase their calculated separation. The major cause of the difference, however, is probably our imposition of the temperature field. In the quasi-vertical case, HR's calculations show that the temperature field and convection interact so as to reduce the buoyancy forces that drive the flow. As HR point out, this effect is particularly large when S is small. The resulting reduction in flow then allows a larger equilibrium X_z.

3.4. *Additional results*

Figure 4 also shows solution curves for the quasi-vertical case for negative S. These solutions are for m restricted to being below the first singularity of Ψ_-. As HR conjectured, the amount of separation continues to diminish with decreasing S. Non-unique solutions exist for $\gamma = 1°$ for S less than about -0.034. Figure 5 shows solution curves for S equal to -0.05 and -0.10. The number of solutions appear to increase steadily with increasing A. It seems likely, however, that all these solutions except the ones shown in figure 4 are unstable. Investigation of solution curves for $|\gamma| < 90°$ for other negative S showed rapidly and widely varying patterns of solutions.

Solutions were also investigaged for various $|\gamma| < 90°$ for positive S. The investigation was limited to $S \leqslant 1$. We found that regions of multiple solutions diminished as γ increased. This, of course, is expected from (3.2), (3.3*b*). For $S \leqslant 1$,

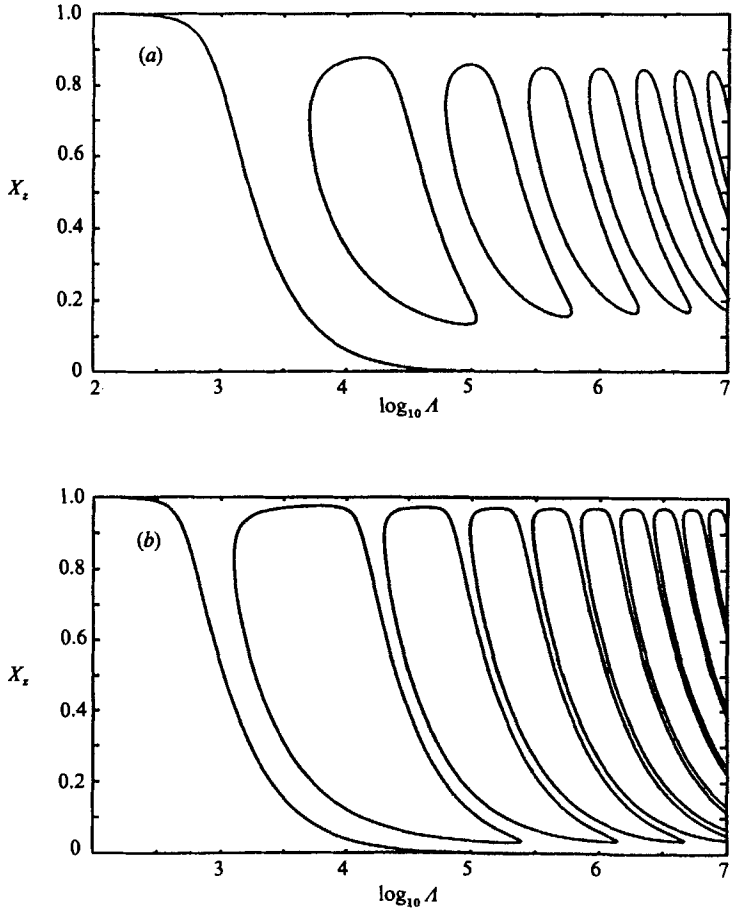

FIGURE 5. $X_z(A)$ for $\gamma = 1°$ for (*a*) $S = -0.05$, (*b*) $S = -0.10$.

multiple solution regions disappear at about $\gamma = 28°$. Figure 6 shows $X_z(A, S)$ for γ equal to 10°, 15°, 20° and 25°.

HR present a number of results for various γ and S at low A. Table 3 compares some of their results to ours. Again, agreement is found to be very good.

4. Concluding comments

Parallel flow solutions, despite their apparent straightforwardness, can still be useful as a research tool. This is particularly true in materials transport problems, where interaction between component gradients and convection can lead to rather complicated phenomena. We have shown that some of HR's numerical results can be matched by fairly simple solutions. The non-uniqueness of these solutions explains some transition phenomena that they observed in the quasi-vertical case. We have uncovered other instances of non-uniqueness that may be worth further investigation.

The existence of multiple solutions brings up the intriguing question of whether more than one can be stable and then to the question of what initial conditions lead

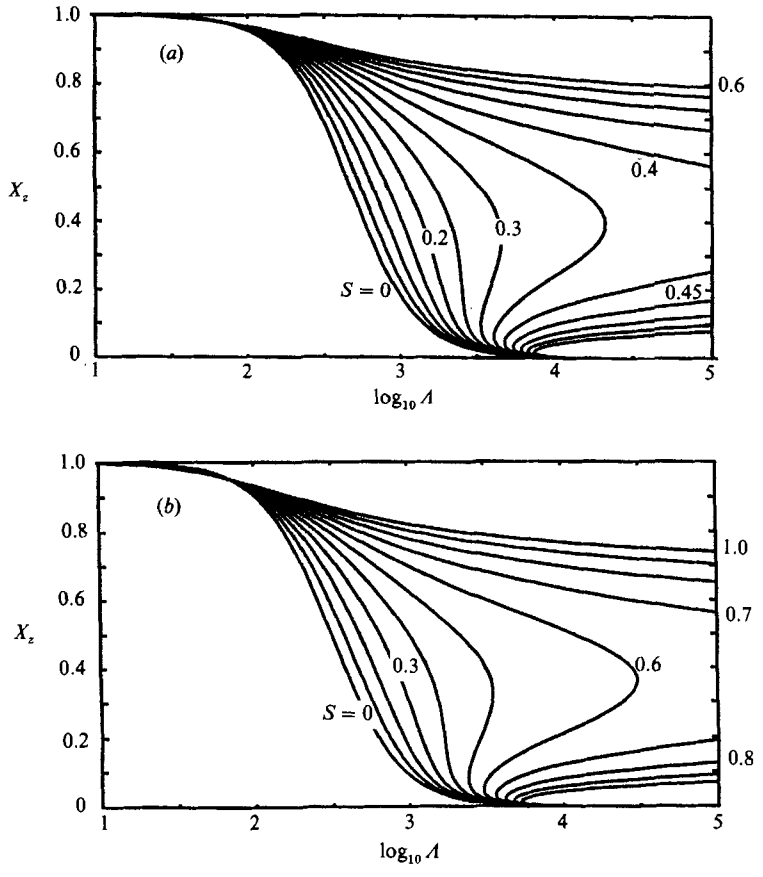

FIGURE 6(*a*, *b*). For caption see facing page.

to one or the other. It may be possible that two such solutions can coexist – that a cylinder can have alternating pockets of different types of flow. Jacqmin (1986, 1989) shows that this type of behaviour occurs in some convection–diffusion systems in porous media. He considered a gravity-segregating oil–gas mixture subject to a horizontal temperature gradient. The precisely analogous situation for Soret diffusion is, for $S > 0$, a horizontal channel cooled from below and subject to a weak horizontal temperature gradient.

In analysing the problem we have chosen the simple course of idealizing the temperature field as imposed. We emphasize that this has been for clarity and that the solution procedure used here can, at least in principle, be applied with an unknown $\{r, \theta\}$ temperature variation and an arbitrary number of components. The key here is that the equation system for the temperature and the components (assuming constant coefficients) is of the form

$$X_{i,z} w_1 = \boldsymbol{A}\left(\frac{\mathrm{d}^2 X_{1,i}}{\mathrm{d}r^2} + \frac{1}{r}\frac{\mathrm{d}X_{1,i}}{\mathrm{d}r} - \frac{1}{r^2} X_{1,i}\right), \tag{4.1}$$

where $\boldsymbol{A}$ is a constant coefficient matrix, T is included in the X_i, and $X_{i,z}$ is the axial gradient of X_i. The $X_{1,i}$ can be decoupled from each other according to

$$\frac{\mathrm{d}^2 X_{1,i}}{\mathrm{d}r^2} + \frac{1}{r}\frac{\mathrm{d}X_{1,i}}{\mathrm{d}r} - \frac{1}{r^2} X_{1,i} = \boldsymbol{A}^{-1} X_{i,z} w_1. \tag{4.2}$$

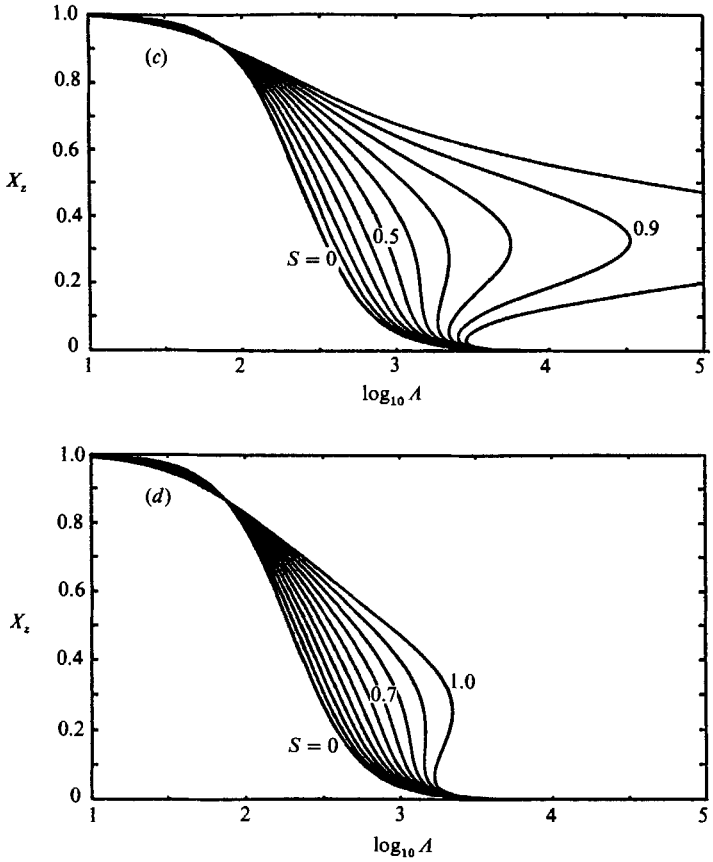

FIGURE 6. $X_z(A)$ for (*a*) $\gamma = 10°$, (*b*) $\gamma = 15°$, (*c*) $\gamma = 20°$, and (*d*) $\gamma = 25°$. S for (*a*) is from 0 to 0.6 by intervals of 0.05. S for (*b–d*) is from 0 to 1 by intervals of 0.1.

The fourth-order equation for w_1 becomes

$$\left(\frac{\mathrm{d}^2}{\mathrm{d}r^2}+\frac{1}{r}\frac{\mathrm{d}}{\mathrm{d}r}-\frac{1}{r^2}\right)^2 w_1+g_z\Big(\sum_i S_i \boldsymbol{A}^{-1}X_{i,z}\Big)w_1 = 0. \tag{4.3}$$

If T is fixed on the walls then T_1 and w_1 are coupled through the boundary conditions. If the walls are insulated then the boundary conditions for w_1 are the same as for equations (2.4). In either case, once T_1 and w_1 are solved for, the remaining $X_{1,i}$ can be found one by one. The $X_{i,z}$ can then be determined by solving the resulting no-flux equations.

REFERENCES

ABRAMOWITZ, M. & STEGUN, I. A. 1964 *Handbook of Mathematical Functions*. US Government Printing Office.

HART, J. E. 1971 On sideways diffusive instability. *J. Fluid Mech.* **49**, 279–288.

HENRY, D. & ROUX, B. 1986 Three-dimensional numerical study of convection in a cylindrical diffusion cell: its influence on the separation of constituents. *Phys. Fluids* **29**, 3562–3572.

HENRY, D. & ROUX, B. 1987 Three dimensional numerical study of convection in a cylindrical diffusion cell: inclination effect. *Phys. Fluids* **30**, 1656–1666.

HENRY, D. & ROUX, B. 1988 Soret separation in a quasi-vertical cylinder. *J. Fluid Mech.* **195**, 175–200.

JACQMIN, D. 1986 Convection of a gravity segregating fluid forced by a horizontal temperature gradient: An energy stability analysis. In *Mathematics Applied to Fluid Mechanics and Stability*, pp. 263–273. SIAM.

JACQMIN, D. 1989 The interaction of natural convection and gravity segregation in oil-gas reservoirs. *Reservoir Engng* (to appear).

PALIWAL, R. C. & CHEN, C. F. 1980 Double-diffusive instability in an inclined fluid layer. Part 2. Stability analysis. *J. Fluid Mech.* **98**, 769–785.